11-14-2016

Selective Growth of Epitaxial Sr_2IrO_4 by Controlling Plume Dimensions in Pulsed Laser Deposition

Sung S. Ambrose Seo
University of Kentucky, a.seo@uky.edu

J. Nichols
University of Kentucky

J. Hwang
The Ohio State University

Jsaminka Terzic
University of Kentucky, jasminka.terzic@uky.edu

John H. Gruenewald
University of Kentucky, john.gruenewald@uky.edu

See next page for additional authors

Tuning the photovoltaic effect of multiferroic $CoFe_2O_4$/Pb(Zr, Ti)O_3 composite films by magnetic fields

Dan-Feng Pan, Guang-Yi Chen, Gui-Feng Bi, Hao Zhang, Jun-Ming Liu, Guang-Hou Wang, and Jian-Guo Wan

Citation: Appl. Phys. Lett. **108**, 222902 (2016);
View online: https://doi.org/10.1063/1.4953154
View Table of Contents: http://aip.scitation.org/toc/apl/108/22
Published by the American Institute of Physics

Tuning the photovoltaic effect of multiferroic $CoFe_2O_4$/Pb(Zr, Ti)O_3 composite films by magnetic fields

Dan-Feng Pan,[1] Guang-Yi Chen,[1] Gui-Feng Bi,[1] Hao Zhang,[2] Jun-Ming Liu,[1,3] Guang-Hou Wang,[1,3] and Jian-Guo Wan[1,3,a)]

[1]*National Laboratory of Solid State Microstructures and Department of Physics, Nanjing University, Nanjing 210093, China*
[2]*Department of Physics and Astronomy, University of Kentucky, Lexington, Kentucky 40506-0055, USA*
[3]*Collaborative Innovation Center of Advanced Microstructures, Nanjing University, Nanjing 210093, China*

(Received 4 January 2016; accepted 20 May 2016; published online 1 June 2016)

The 0–3 type $CoFe_2O_4$-Pb(Zr,Ti)O_3 (CFO-PZT) multiferroic composite films have been prepared by a sol-gel process and spin-coating technique. A confirmable photovoltaic effect is observed under ultraviolet light irradiation. Moreover, this photovoltaic effect can be tuned by external magnetic fields. The maximum magnetic modulation ratios of short-circuit current density and open-circuit voltage can reach as high as 13.7% and 12.8% upon the application of 6 kOe DC magnetic field. Through remnant polarization measurements under various magnetic fields and detailed analysis of the energy band structures, we elucidate the mechanism of tuning photovoltaic effect by magnetic fields and attribute it to the combination of two factors. One is the decreased ferroelectric-polarization-induced depolarization electric field and another is the band structure reconstruction at CFO-PZT interfaces, both of which are dominated by the magnetoelectric coupling via interfacial stress transferring at nanoscale. This work makes some attempts of coupling photo-induced effects with magnetoelectric effect in multiferroic materials and will widen the practical ranges of multiferroic-based applications. *Published by AIP Publishing.*
[http://dx.doi.org/10.1063/1.4953154]

Recently, ferroelectric oxides have received much attention in solar energy conversion areas such as solar cell,[1] photocatalytic,[2] and photo-electro-chemical water splitting.[3] The ferroelectric photovoltaic effect shares a large above-bandgap open-circuit voltage,[4] which points to the ferroelectric-polarization-driven carrier separation mechanism fundamentally different from that of traditional semiconductor p-n junctions. However, such a focus on only photovoltaics is too restrictive and more attention should be paid to explore other valuable applications.[5] For example, the switchable photovoltaic effect in some ferroelectric materials (e.g., $BiFeO_3$)[6] can be used to sense the polarization direction non-destructively in ferroelectric memory units,[7] and the ferroelectric thin films with in-plane polarization configuration can also be utilized to develop high-sensitive and fast-response photodetectors.[8] Besides, the introduction of light into ferroelectrics gives us extra freedom to couple the ferroelectric polarization with other physical properties such as deformation,[9] domain walls,[4] and polymorphic phase interfaces.[10]

It is noteworthy that some ferroelectrics are included in the multiferroics, which naturally possess the coupling of multiple ferroic orders (e.g., ferroelectricity, ferroelasticity, and ferromagnetism).[11,12] The extra light irradiation in multiferroics will inevitably come across an abundance of interesting physics and possible practical applications. Current research about the photovoltaic effect in multiferroic area mainly concentrate on the light-induced electromechanical properties. Nevertheless, the coupling between light and magnetic properties has seldom been studied. Moreover, the multi-field manipulation of photovoltaic effect has become an interesting topic in current multifunctional applications, e.g., the magnetic tuning of photovoltaic effect in silicon-based Schottky junctions,[13] the magneto-tunable photocurrent in manganite-based heterojunctions,[14] and magnetic field effects in hybrid perovskites $CH_3NH_3PbI_{3-x}Cl_x$.[15] Yet, tuning the photovoltaic effect by magnetic fields in multiferroic materials has not been realized. The reason may be that the intrinsic magnetoelectric coupling in single phase multiferroics is too weak.[16] Very differently, multiferroic composite materials, which are composed of independent ferroelectric and ferromagnetic materials through a certain phase connection, usually possess a large magnetoelectric coupling by interfacial stress transferring.[17,18] Such a strong magnetoelectric coupling between ferroelectric and ferromagnetic phases perhaps provides a promising avenue to realize a considerable magnetic tuning of photovoltaic effect.

In this work, we report on a remarkable magnetic tuning of photovoltaic effect in the 0–3 type $CoFe_2O_4$-Pb(Zr,Ti)O_3 (CFO-PZT) multiferroic composite films. Both short-circuit current density (J_{SC}) and open-circuit voltage (V_{OC}) can be controllably tuned with external magnetic fields. Under 6 kOe DC magnetic field, the maximum magnetic modulation ratios (γ^H) of J_{SC} and V_{OC} can reach 13.7% and 12.8%, respectively. Based on the analysis of the change in the ferroelectric polarization behaviors and the energy band structures under external magnetic fields, we have revealed the mechanism of magnetic tuning of photovoltaic effect and

a)Author to whom correspondence should be addressed. Electronic mail: wanjg@nju.edu.cn

attribute it to the variation of the net depolarization field and the reconstruction of interfacial band structures at CFO-PZT interfaces, both of which are caused by the magnetoelectric coupling in the composite films.

The 0–3 type CFO-PZT multiferroic composite films were deposited on the commercial Pt/Ti/SiO_2/Si(100) substrates by a typical sol-gel process and spin-coating technique. A 0.2 mol/l solution of CFO (with a molar ratio of Co^{2+}:Fe^{3+} = 1:2) and a 0.2 mol/l solution of PZT (with a molar ratio of Zr:Ti = 52:48 and 10 mol. % excess Pb^{2+}) were used, in which acetic acid and 2-methoxyethanol (1:4, volume ratio) were chosen as mixture solvents. These two sol solutions were alternately spin-coated onto the substrate so as to form a precursor composite film, consisting of four PZT layers and two CFO layers. After that, the precursor composite film was calcined at 650 °C for 5 min under oxygen atmosphere by the rapid annealing process, accompanied with a deep diffusion between PZT and CFO phases. The detailed preparation can also be found elsewhere.[19]

The phase structure characterizations of the composite films were carried out by x-ray diffraction (XRD) analysis on a D/MAX-RA diffractometer with Cu Kα radiation. Only polycrystalline PZT and CFO phases were observed and no impurity phase was found. The cross sectional morphology examined by scanning electron microscopy (SEM, LEO-1530VP) determined the thickness of the composite film to be ~200 nm (Figure S1(a) in the supplementary material[33]). We also performed magnetic and ferroelectric polarization hysteresis loop tests using a superconducting quantum interference device (SQUID, Quantum Design) and a ferroelectric analyzer (Precision Multiferroic, Radiant Inc.). The composite film exhibits both evident ferromagnetic and ferroelectric characteristics, as depicted in Figure S1(b) of the supplementary material.[33] To confirm the phase connection type of the composite film, the surface morphology was measured with a semi-contact atomic force microscopy (AFM, NT-MDT Inc.). As shown in Figure 1(a), the cubic nanoparticles are uniformly embedded in the matrix, indicating a 0–3 type phase connection. The average size of the particles is ~100 nm. The further magnetic structure characterization using a magnetic force microscopy (MFM, attached to AFM) in Figure 1(b) indicates that these nanoparticles are magnetic CFO phases. According to the above analysis, we believe that the composite film has a 0–3 type phase connection, i.e., the magnetic CFO nanoparticles are uniformly distributed in the ferroelectric PZT matrix.

The photovoltaic effect was performed with a self-made apparatus shown in the inset of Figure 1(c). Since the optical bandgap of the composite film was determined to be 3.48 eV by the Tauc's equation[20] (Section II of the supplementary material[33]), we used the ultraviolet (UV) lights to irradiate the film. The incident UV light was generated by a 300 W UV-enhanced Xe lamp equipped with a UV reflector plate and its intensity was set to be 60 mW/cm^2. Considering that thin Pt film is UV semitransparent,[21] we deposited a 40 nm-thick Pt layer onto the composite film as top electrode by magnetron sputtering. All the photovoltaic signals, including dark leakage-current, open-circuit voltage, and short-circuit current, were recorded by a Keithley 6517B electrometer with an aluminum shielding box ensuring a careful

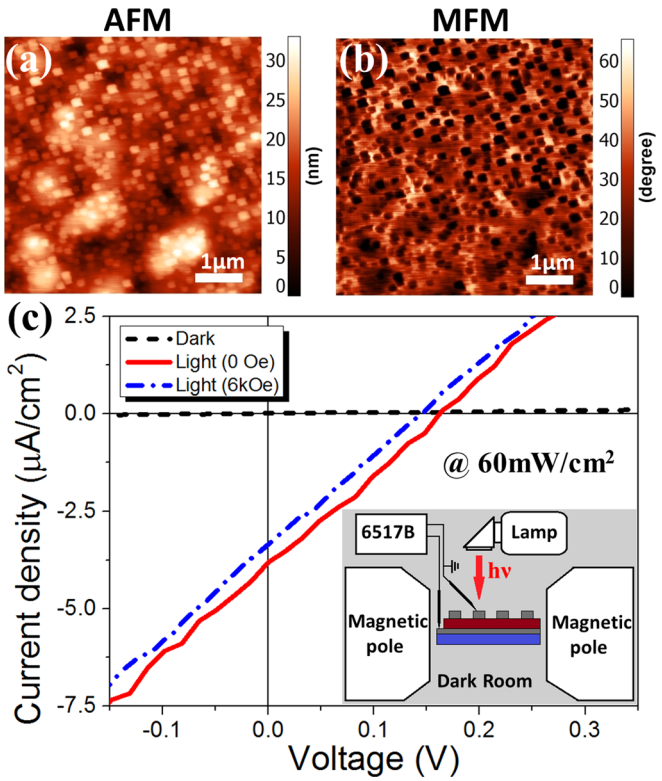

FIG. 1. (a) Surface AFM image and (b) surface MFM image for the composite film. (c) Photovoltaic current density vs voltage ($J-V$) curves of the composite film under dark, light (0 Oe) and light (6 kOe) circumstances, respectively. The inset gives a sketch map of the measurement apparatus.

electromagnetic isolation. Figure 1(c) shows the photovoltaic current density vs voltage ($J-V$) characteristics of the composite film. The black dashed and the red solid lines represent the typical photovoltaic $J-V$ curves under dark and light circumstances, respectively. Accordingly, J_{SC} = 3.840 μA/cm^2 and V_{OC} = 0.164 V were obtained, indicative of confirmable photovoltaic effect under UV light illumination (Section III of the supplementary material[33]). Then we applied a 6 kOe DC magnetic field supported by an electromagnet and repeatedly carried out $J-V$ measurements, as shown in the blue dashed dotted line of Figure 1(c). The results show that external magnetic fields can give rise to an evident change in the photovoltaic effect. For instance, J_{SC} decreases to 3.312 μA/cm^2 while V_{OC} drops to 0.143 V upon the application of 6 kOe DC magnetic field.

Subsequently, the influence of the magnetic field strength on the photovoltaic effect of the composite film was systematically studied by carrying out photovoltaic $J-V$ measurements under various magnetic fields. It is worth mentioning that the photovoltaic process inevitably brings about thermal effect,[22] which can inspire more electrons jumping into the conduction bands of the absorbing layer and interfere with the accuracy of this experiment. Therefore, we also independently performed the time-dependent photovoltaic tests without applying magnetic fields in order to examine the influence of thermal effect. The sequences of applying magnetic field (H) and time-points of measuring photovoltaic $J-V$ curves are plotted in Figure 2(c). After each applied magnetic field was stabilized for 1 min, the photovoltaic $J-V$ test was performed for 5 s. Note that the time sequence

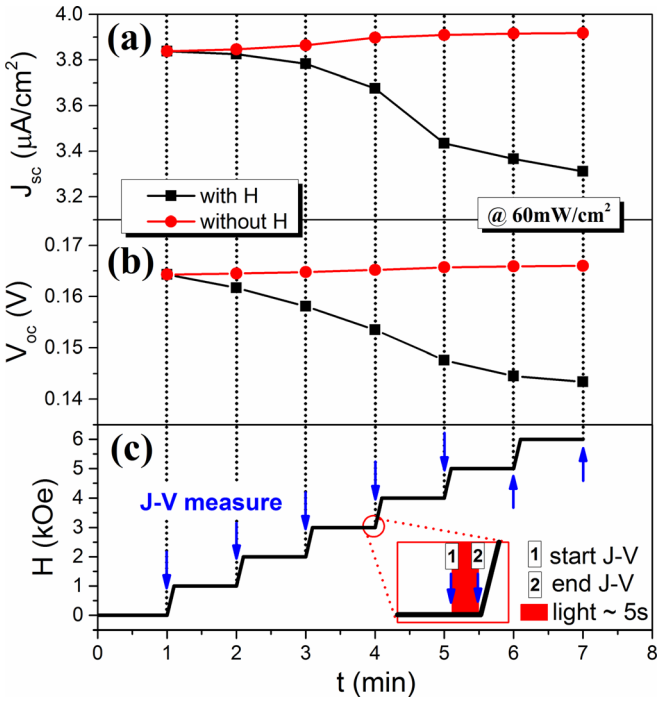

FIG. 2. (a) J_{SC} and (b) V_{OC} values extracted from the corresponding $J-V$ curves measured under various DC magnetic fields (H) or without H with the same time interval. Note that the thermal effect tests were carried out in the absence of magnetic fields. (c) The sequence diagram of applying magnetic field and measuring $J-V$ curves. The magnified image gives the detailed time-points of the $J-V$ measurements, including the start $J-V$ point, end $J-V$ point, and the illumination time ~5 s.

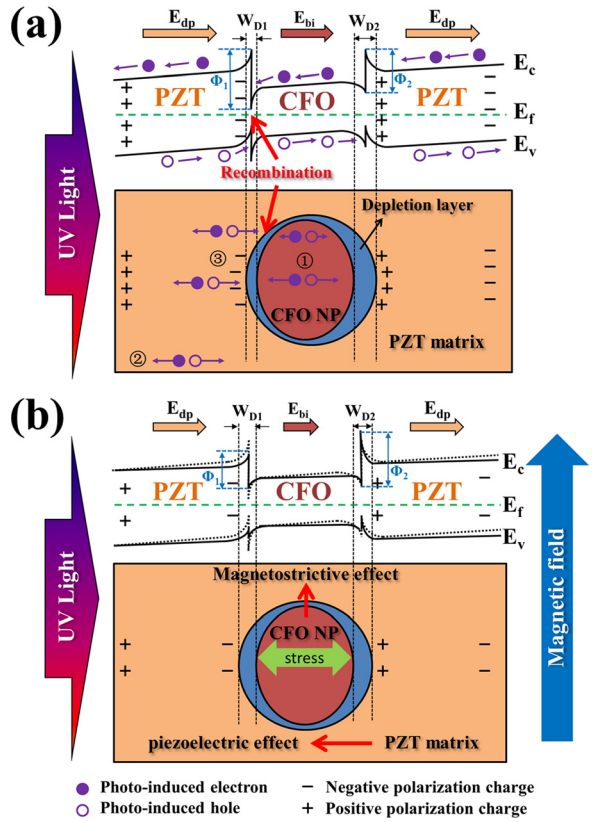

FIG. 3. (a) The simplified diagram of the energy band structure for a typical unit before being subjected to the external magnetic fields (top part) and the illustration of generation, separation, transportation of photo-induced carriers in the composite film (bottom part). Two Pt electrodes are short-circuited under UV irradiation. Note that the energy band model and all discussions are based on the assumption of p-type CFO and PZT. (b) The corresponding schematic drawings of the sample after being subjected to external magnetic fields.

of thermal effect tests (i.e., $J-V$ measurements without H) is exactly the same as that of applying magnetic fields. Figures 2(a) and 2(b) show J_{SC} and V_{OC} values derived from corresponding $J-V$ curves as a function of time (t) with and without H, respectively. Upon the application of external magnetic field, both J_{SC} and V_{OC} decrease with increasing the magnetic field. Without applying magnetic fields, however, both J_{SC} and V_{OC} increase slightly with increasing the measuring time. The above results make it a robust viewpoint that external magnetic fields truly have a great influence on the photovoltaic effect.

In order to understand the photovoltaic process and its response to external magnetic fields for the composite film, we chose a typical unit and drew the schematic energy band structure as well as the corresponding illustration of the photo-induced carriers' emotion process under the UV light irradiation, as shown in Figure 3(a). When reaching a thermal dynamic equilibrium, a depletion layer surrounding the CFO nanoparticle is formed due to the difference of energy band structures between CFO and PZT. Here, we assume that both PZT and CFO are p-type semiconductors,[23,24] so the Fermi energy level is closer to the valence band. The optical bandgap of CFO[25] is smaller than that of PZT, which explains the smaller bandgap of the composite film ~3.48 eV compared with the pure PZT film ~3.60 eV (Figure S2(b), supplementary material[33]). Because of the high electron affinity of CFO[26] mismatching with PZT, a high interfacial barrier is produced. Moreover, due to the existence of ferroelectric polarization in the PZT matrix, the induced depolarization field manifests itself in both conductive band and valance band as a slope.[27] The positive majority free carriers in the CFO nanoparticle is attracted (or repelled) by the negative (or positive) polarization bound charges of the PZT matrix to the CFO-PZT interfaces. This leads to the formation of additional built-in electric field (E_{bi}) in the CFO nanoparticle with the same direction of the depolarization field (E_{dp}) in the PZT matrix, accompanied with the formation of asymmetric interfacial barrier heights (Φ_1 and Φ_2) and depletion layer widths (W_{D1} and W_{D2}) at two sides of the CFO-PZT interfaces, as shown in Figure 3(a).

Accordingly, it is considered that the introduction of CFO nanoparticles makes the energy band structure of the composite film different from the pure PZT, causing a change in the photovoltaic process including the generation, separation, and transportation of the photo-induced carriers. When the composite film is irradiated by incident UV lights, both CFO nanoparticles and PZT matrix can produce an abundance of photo-induced carriers. The photo-induced electrons will jump into the respective conductive bands, leaving the photo-induced holes in relevant valance bands.[28] Afterwards, the photo-induced carriers are separated by both E_{dp} in PZT and E_{bi} in CFO to the opposite direction. For the photo-induced carriers generated in CFO nanoparticles (position 1), the high interfacial barriers between CFO and PZT block them from crossing the interfaces into the PZT matrix (Section V of the supplementary material[33]). These carriers have to accumulate at the CFO surfaces, some of which

annihilate each other. For the photo-induced carriers generated in PZT matrix, on the one hand, the transportation of the carriers in position 2 (far away from CFO) is not influenced by CFO and these carriers can pass through the PZT matrix to the outside circuit. On the other hand, the photo-induced carriers generated in position 3 (near the CFO surfaces) can be easily trapped at the CFO surfaces because of the badly band bending[29] at the CFO-PZT interfaces. Moreover, the recombination with a big probability through the tunneling effect[30] may occur between the photo-induced carriers in CFO nanoparticles and PZT matrix. Note that the number of trapped photo-induced carriers depends on the interfacial barrier height and the probability of carrier recombination is related to the interfacial layer width. Therefore, the combination influence of the above two factors provides us more freedom, making it possible to tune the photovoltaic process by changing band structure under external magnetic fields through magnetoelectric coupling.

To further understand how the photovoltaic effect is tuned by external magnetic fields, we measured two-fold remnant polarization (P_r) values of the composite film under various magnetic fields by the standard five-pulse positive-up negative-down (PUND) method[31] (Section VII of the supplementary material[33]). Figure 4(c) plots the $2P_r$ values as a function of applied magnetic field (H). It turns out that the $2P_r$ value decreases with increasing H and becomes saturated when H is large enough, which is in accordance with the typical magnetoelectric coupling process caused by interfacial stress transferring.[17] To obtain accurate relations between photovoltaic parameters (i.e., J_{SC} and V_{OC}) and H, we deduct the influence of thermal effect on the magnetic tuning of photovoltaic effect in Figure 2. After removing the thermal effect, the true photovoltaic parameters affected by H can be expressed as follows:

$$\Delta PV = PV_{(magnetic\,field)} - \left(PV_{(thermal\,effect)} - PV_{H=0}\right), \quad (1)$$

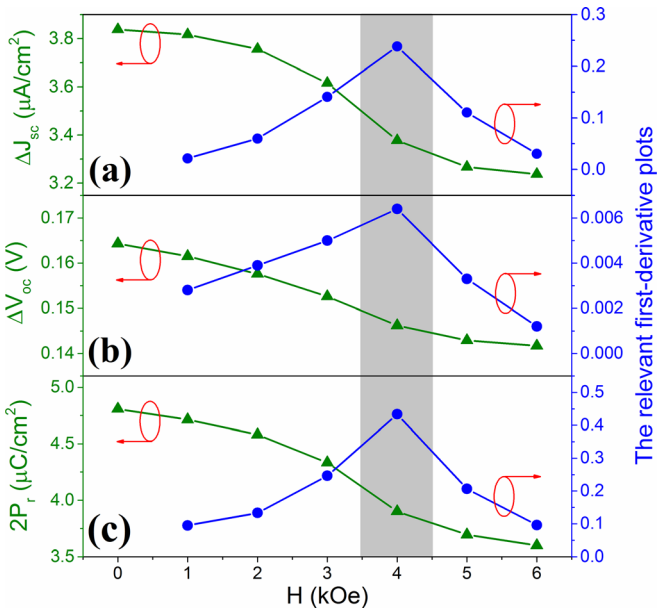

FIG. 4. (a) ΔJ_{SC}, (b) ΔV_{OC}, and (c) $2P_r$ values as a function of applied magnetic field (H). The right-hand side of the figure gives the corresponding first-derivative plots to H.

where PV means the photovoltaic parameters J_{SC} or V_{OC}, $PV_{H=0}$ is the corresponding J_{SC} or V_{OC} values at zero magnetic field, $PV_{(magnetic\,field)}$ and $PV_{(thermal\,effect)}$ represent the photovoltaic parameters with magnetic field and thermal effect, respectively. Through the calculation based on Eq. (1), we plotted ΔJ_{SC} and ΔV_{OC} as a function of H, as shown in Figures 4(a) and 4(b). It is obvious that the variation tendencies of both ΔJ_{SC} and ΔV_{OC} with H are the same as that of $2P_r$. The further first-derivative plot of Figure 4(c) actually reflects the variation of magnetoelectric coupling strength with the external magnetic fields,[32] which turns out the strongest magnetoelectric effect at so-called optimized magnetic field ~4 kOe. The first-derivative plots of ΔJ_{SC} and ΔV_{OC} to H in Figures 4(a) and 4(b) show the same optimized magnetic field ~4 kOe. Therefore, we conclude that the magnetic tuning of photovoltaic effect in the composite film is exactly dominated by the magnetoelectric coupling via interfacial stress transferring between ferroelectric PZT and ferromagnetic CFO. We also excluded the possible situations of the magnetic-field-induced localization of carriers at defects or the traditional Hall effect (Section VI of the supplementary material[33]). Here, we define the magnetic modulation ratio of photovoltaic parameters as

$$\gamma_{PV}^{H} = \frac{PV_H - PV_0}{PV_0}, \quad (2)$$

where PV is the photovoltaic parameters (i.e., J_{SC} and V_{OC}), H means the applied magnetic field, PV_H represents the corresponding photovoltaic parameter values at a fixed magnetic field H, and PV_0 is the photovoltaic parameter value at $H = 0$. The calculated maximum $\gamma_{J_{SC}}^{H}$ and $\gamma_{V_{OC}}^{H}$ values reach 13.7% and 12.8% at $H = 6.0$ kOe, respectively.

The magnetic tuning of photovoltaic effect in the composite film can also be well understood based on the analysis of the change in the energy band structures under magnetic fields. As shown in Figure 3(b), upon the application of external magnetic fields, the ferroelectric polarization of the composite film becomes smaller due to the magnetoelectric effect. In detail, the magnetoelectric coupling starts from the magnetostrictive effect of the CFO nanoparticles induced by external magnetic fields, which is further transferred to the PZT matrix via the interfacial stress-transferring and finally weakens the ferroelectric polarization in PZT due to the piezoelectric effect. So the polarization-induced E_{dp} in the PZT matrix becomes weak, making the separation of photo-induced carriers in position 2 get harder and reducing the interfacial bound polarization charges. As a result, the accumulated (or depleted) positive majority free carriers in CFO are partly released (or compensated), leading to the decrease of E_{bi}. At the same time, W_{D1} becomes wider while Φ_1 gets lower, meanwhile W_{D2} becomes narrower while Φ_2 gets higher, consequently causing the change in the number of trapped photo-induced carriers and the probability of carrier recombination. Both the decreased E_{dp} and reconstructed interfacial band structures caused by the magnetoelectric coupling effect via the interfacial stress-transferring make the separation of photo-induced carriers become harder, leading to the decrease of J_{SC} and V_{OC} upon the application of external magnetic fields (Figures 4(a) and 4(b)).

In summary, we have fabricated the 0–3 type CFO-PZT multiferroic composite films exhibiting evident photovoltaic effect under UV light irradiation and realized the magnetic tuning of photovoltaic effect in such composite films. It was experimentally confirmed that the variation tendencies of photovoltaic parameters under external magnetic fields were almost the same as that of the ferroelectric remnant polarization, strongly suggesting that the magnetoelectric coupling between ferroelectric PZT matrix and ferromagnetic CFO nanoparticles should be responsible for the magnetic tuning of photovoltaic effect. Further analysis of energy band structures revealed that the change in depolarization fields of the composite film and the reconstruction of band structures at CFO-PZT interfaces played important roles in the magnetic tuning of photovoltaic effect. Our present work provides a valuable guide for basic research of multiferroic materials with multi-field coupling effects and offers instructive ideas for developing multifunctional devices.

This work was supported by the National Key Projects for Basic Research of China (Grant No. 2015CB921203), the National Natural Science Foundation of China (Grant Nos. 51472113 and 11134005), and the PAPD Project.

[1]R. Nechache, C. Harnaagea, S. Li, L. Cardenas, W. Huang, J. Chakrabartty, and F. Rosei, Nat. Photonics **9**, 61 (2015).
[2]M. Sakar, S. Balakumar, P. Saravanan, and S. Bharathkumar, Nanoscale **8**, 1147 (2016).
[3]W. G. Yang, Y. H. Yu, M. B. Starr, X. Yin, Z. D. Li, A. Kvit, S. F. Wang, P. Zhao, and X. D. Wang, Nano Lett. **15**, 7574 (2015).
[4]S. Y. Yang, J. Seidel, S. J. Byrnes, P. Shafer, C. H. Yang, M. D. Rossell, P. Yu, Y. H. Chu, J. F. Scott, J. W. Ager III, L. W. Martin, and R. Ramesh, Nat. Nanotechnol. **5**, 143 (2010).
[5]Y. Sharma, P. Misra, R. K. Katiyar, and R. S. Katiyar, J. Phys. D: Appl. Phys. **47**, 425303 (2014).
[6]R. Agarwal, Y. Sharma, and R. S. Katiyar, Appl. Phys. Lett. **107**, 162904 (2015).
[7]R. Guo, L. You, Y. Zhou, Z. S. Lim, X. Zou, L. Chen, R. Ramesh, and J. L. Wang, Nat. Commun. **4**, 1990 (2013).
[8]J. Xing, E. J. Guo, J. J. Dong, H. Y. Hao, Z. Y. Zheng, and C. C. Zhao, Appl. Phys. Lett. **106**, 033504 (2015).
[9]B. Kundys, M. Viret, D. Colson, and D. O. Kundys, Nat. Mater. **9**, 803 (2010).
[10]K. Chu, B. K. Jang, J. H. Sung, Y. A. Shin, E. S. Lee, K. Song, J. H. Lee, C. S. Woo, S. J. Kim, S. Y. Choi, T. Y. Koo, Y. H. Kim, S. H. Oh, M. H. Jo, and C.-H. Yang, Nat. Nanotechnol. **10**, 972 (2015).
[11]W. Eerenstein, N. D. Mathur, and J. F. Scott, Nature **442**, 759 (2006).
[12]R. Ramesh and N. A. Spaldin, Nat. Mater. **6**, 21 (2007).
[13]S. H. Wang, W. X. Wang, L. K. Zou, X. Zhang, J. W. Cai, Z. G. Sun, B. G. Shen, and J. R. Sun, Adv. Mater. **26**, 8059 (2014).
[14]Z. G. Sheng, M. Nakamura, W. Koshibae, T. Makino, Y. Tokura, and M. Kawasaki, Nat. Commun. **5**, 4584 (2014).
[15]C. Zhang, D. Sun, C. X. Sheng, Y. X. Zhai, K. Mielczarek, A. Zakhidov, and Z. V. Vardeny, Nat. Phys. **11**, 427 (2015).
[16]R. Seshadri and N. A. Hill, Chem. Mater. **13**, 2892 (2001).
[17]J. Ma, J. M. Hu, Z. Li, and C. W. Nan, Adv. Mater. **23**, 1062 (2011).
[18]C. W. Nan, M. I. Bichurin, S. X. Dong, D. Viehland, and G. Srinivasan, J. Appl. Phys. **103**, 031101 (2008).
[19]J. G. Wan, X. W. Wang, Y. J. Wu, M. Zeng, Y. Wang, H. Jiang, W. Q. Zhou, G. H. Wang, and J. M. Liu, Appl. Phys. Lett. **86**, 122501 (2005).
[20]J. Tauc, Mater. Res. Bull. **5**, 721 (1970).
[21]F. G. Zheng, J. Xu, L. Fang, M. R. Shen, and X. L. Wu, Appl. Phys. Lett. **93**, 172101 (2008).
[22]T. Choi, S. Lee, Y. J. Choi, V. Kiryukhin, and S. W. Cheong, Science **324**, 63 (2009).
[23]Y. Watanabe, Phys. Rev. B **57**, R5563 (1998).
[24]G. H. Jonker, Phys. Chem. Solids **9**, 165 (1959).
[25]D. Sharma and N. Khare, Appl. Phys. Lett. **105**, 032404 (2014).
[26]C. Borgohain, K. K. Senapati, K. C. Sarma, and P. Phukan, J. Mol. Catal. A: Chem. **363–364**, 495 (2012).
[27]J. Shi, M. B. Starr, and X. D. Wang, Adv. Mater. **24**, 4683 (2012).
[28]C. R. Bowen, H. A. Kim, P. M. Weaver, and S. Dunn, Energy Environ. Sci. **7**, 25 (2014).
[29]B. C. Huang, Y. T. Chen, Y. P. Chiu, Y. C. Huang, J. C. Yang, Y. C. Chen, and Y. H. Chu, Appl. Phys. Lett. **100**, 122903 (2012).
[30]D. W. Cao, C. Y. Wang, F. G. Zheng, W. Dong, L. Fang, and M. R. Shen, Nano Lett. **12**, 2803 (2012).
[31]B. Chen, J. Y. Wang, M. X. Zhou, J. G. Wan, and J. M. Liu, J. Am. Ceram. Soc. **97**, 1450 (2014).
[32]H. C. Miao, X. L. Zhou, S. X. Dong, H. S. Luo, and F. X. Li, Nanoscale **6**, 8515 (2014).
[33]See supplementary material at http://dx.doi.org/10.1063/1.4953154 for XRD pattern, cross sectional SEM image, and other supplied experimental results.